



OPEN ACCESS

EDITED BY

Berislav Buca,
University of Copenhagen, Denmark

REVIEWED BY

Pragya Shukla,
Indian Institute of Technology Kharagpur, India
Abolfazl Bayat,
University of Electronic Science and
Technology of China, China

*CORRESPONDENCE

Samuel L. Jacob,
✉ samjac91@gmail.com

RECEIVED 31 July 2024

ACCEPTED 25 September 2024

PUBLISHED 22 October 2024

CITATION

Jacob SL, Bettmann LP, Lacerda AM,
Zawadzki K, Clark SR, Goold J and
Mendoza-Arenas JJ (2024) Dephasing-assisted
transport in a tight-binding chain with a
linear potential.

Front. Phys. 12:1474018.

doi: 10.3389/fphy.2024.1474018

COPYRIGHT

© 2024 Jacob, Bettmann, Lacerda, Zawadzki,
Clark, Goold and Mendoza-Arenas. This is an
open-access article distributed under the terms
of the [Creative Commons Attribution License
\(CC BY\)](https://creativecommons.org/licenses/by/4.0/). The use, distribution or reproduction in
other forums is permitted, provided the original
author(s) and the copyright owner(s) are
credited and that the original publication in this
journal is cited, in accordance with accepted
academic practice. No use, distribution or
reproduction is permitted which does not
comply with these terms.

Dephasing-assisted transport in a tight-binding chain with a linear potential

Samuel L. Jacob^{1*}, Laetitia P. Bettmann¹, Artur M. Lacerda¹,
Krissia Zawadzki², Stephen R. Clark³, John Goold^{1,4} and
Juan José Mendoza-Arenas^{3,5,6}

¹School of Physics, Trinity College Dublin, College Green, Dublin, Ireland, ²Instituto de Física de São Carlos, Universidade de São Paulo, São Paulo, Brazil, ³H. H. Wills Physics Laboratory, University of Bristol, Bristol, United Kingdom, ⁴Trinity Quantum Alliance, Unit 16, Trinity Technology and Enterprise Centre, Dublin, Ireland, ⁵Department of Mechanical Engineering and Materials Science, University of Pittsburgh, Pittsburgh, PA, United States, ⁶Department of Physics and Astronomy, University of Pittsburgh, Pittsburgh, PA, United States

An environment interacting with a quantum system can enhance transport through the suppression of quantum effects responsible for localization. In this paper, we study the interplay between bulk dephasing and a linear potential in a boundary-driven tight-binding chain. A linear potential induces Wannier-Stark localization in the absence of noise, while dephasing induces diffusive transport in the absence of a tilt. We derive an approximate expression for the steady-state current as a function of both dephasing and tilt which closely matches the exact solution for a wide range of parameters. From it, we find that the maximum current occurs for a dephasing rate equal to the period of Bloch oscillations in the Wannier-Stark localized system. We also find that the current displays a maximum as a function of the system size, provided that the total potential tilt across the chain remains constant. Our results can be verified in current experimental platforms and represents a step forward in analytical studies of environment-assisted transport.

KEYWORDS

dephasing assisted transport, bloch oscillations, quantum transport, quantum many body, wannier-Stark localization

1 Introduction

The quantum features of an open system interacting with a macroscopic environment are inevitably destroyed in a process known as decoherence [1–3]. However, the notion that the environment is always detrimental for quantum processes—such as information processing and transport—has been challenged for more than a decade, prompted by investigations of quantum effects in biological systems [4–7]. It is now understood that the environment can assist energy transport in non-interacting quantum systems [4–12], an effect which has been experimentally verified in quantum networks of photons [13, 14], trapped ions [15, 16] and superconducting circuits [17]. Although several mechanisms for environment-assisted quantum transport have been proposed and debated [6, 7, 9], a clear mechanism is at play in localized quantum systems—when destructive interference responsible for localization and transport suppression is destroyed by the environment, quantum transport is enhanced. This is indeed the expected impact of environmental coupling on Anderson and Wannier-Stark localization. In Anderson localized systems,

quantum transport is suppressed as a consequence of lattice disorder [18]. On the other hand, Wannier-Stark localization occurs in the presence of a linear lattice potential such as an electric field [19–21]; in this case, coherent (Bloch) oscillations take place within the region of localization [19, 22–24]. Despite the fact that Wannier-Stark localized systems subject to noise have been investigated [25–28], the literature on this subject is still scarce.

Environment-assisted transport can also affect the non-equilibrium transport properties of many-body quantum systems. A common approach to evidence this effect is to drive the quantum system to a non-equilibrium steady state by high temperature reservoirs located at the boundaries [29, 30]. The dephasing effect of the environment renders the transport diffusive, which has been shown to enhance the steady-state current in boundary-driven systems with disorder [31–33] or quasi-periodicity [34] and to modify the transport properties of systems with long-range hopping [35]. Moreover, Markovian boundary-driven non-interacting systems are amenable to analytical treatment even in the presence of dephasing, with exact and approximate solutions of steady-state quantities available for tight-binding chains [31, 32, 36, 37].

In this paper, we study dephasing-assisted transport in a boundary-driven, tight-binding chain with a linear potential. We make use of a steady-state ansatz elaborated in Refs. Žnidarič [31]; Žnidarič and Horvat [32]; Žnidarič [36] to numerically access the relevant steady-state quantities for up to one thousand chain sites. By performing a minimal approximation, we derive an analytical expression for the steady-state current which matches the exact dynamics for a vast range of parameters. From it, we find that the current is maximized at a dephasing rate equal to the period of Bloch oscillations in a Wannier-Stark localized system. We also find that the current displays a maximum as a function of the system size, provided that the total potential tilt across the chain is kept constant. Our results present a significant contribution in the analytics of environment-assisted transport and can be experimentally verified in several platforms.

The paper is organized as follows. In Sec. 2 we introduce the model and the steady-state ansatz used in our study. In Sec. 3 we present and discuss our results for dephasing-assisted transport. In Sec. 4 we present the conclusion and outlook of our work. The Supplementary Material contains technical details referenced throughout the main text.

2 Setup

2.1 The model

We study a non-interacting, one-dimensional lattice of L sites with Hamiltonian given by the XX model

$$H = J \sum_{j=1}^{L-1} (\sigma_j^x \sigma_{j+1}^x + \sigma_j^y \sigma_{j+1}^y) + \sum_{j=1}^L \epsilon_j \sigma_j^z. \quad (1)$$

In Equation 1 $\{\sigma_j^x, \sigma_j^y, \sigma_j^z\}_{j=1}^L$ are Pauli matrices, J is the hopping term and ϵ_j is a local field which will be specified shortly. In order to induce a non-equilibrium state in the system, we couple the boundary sites to high-temperature reservoirs with different

chemical potentials; in addition, each site is also exposed to its own local reservoir which induces dephasing. All the reservoirs are assumed to be ideal and couple weakly to the system. The dynamics of the system's density operator $\rho(t)$ at time t is given by the Lindblad master equation [2, 3, 30].

$$\frac{d\rho(t)}{dt} = -\frac{i}{\hbar} [H, \rho(t)] + \sum_{\alpha=l,r,d} \mathcal{L}^\alpha[\rho(t)]. \quad (2)$$

Here the superoperator \mathcal{L}^α describes dissipation induced by the reservoirs $\alpha = l, r, d$ corresponding to left boundary, right boundary and dephasing, respectively. It is a sum of local Lindblad jump operators of the form

$$\mathcal{L}^\alpha[\cdot] = \sum_{j,\beta} L_j^{\alpha\beta} \cdot L_j^{\alpha\beta\dagger} - \frac{1}{2} \{L_j^{\alpha\beta\dagger} L_j^{\alpha\beta}, \cdot\}, \quad (3)$$

where j in Equation 3 labels the site acted on by the reservoir α and β labels different jump operators on that same site. The effect of each boundary reservoir ($\alpha = l, r$) is represented by two jump operators

$$L_1^{\pm} = \sqrt{\frac{\Gamma(1 \pm f)}{2}} \sigma_1^\pm, \quad L_L^{\pm} = \sqrt{\frac{\Gamma(1 \mp f)}{2}} \sigma_L^\pm, \quad (4)$$

where Γ in Equation 4 is the coupling rate at the boundaries, f is the chemical potential bias and $\sigma_j^\pm = (\sigma_j^x \pm i\sigma_j^y)/2$. For forward bias ($0 \leq f \leq 1$) excitations are mostly created on the first site and annihilated on the last site; the opposite reasoning applies for reverse bias ($-1 \leq f \leq 0$). In order to describe the effects of dephasing, we consider L jump operators acting on individual sites as if each of them were coupled to its own reservoir

$$L_j^d = \sqrt{\frac{\gamma}{2}} \sigma_j^z, \quad j = 1, 2, \dots, L, \quad (5)$$

where γ in Equation 5 is the dephasing rate.

The key observables in the system are the magnetization and its associated current. We denote by $\langle A \rangle(t) \equiv \text{Tr}[A\rho(t)]$ the expectation value of an observable A at time t . Differentiating with respect to time and using Equation 2 yields a continuity equation (see Supplementary Material for more details)

$$\begin{aligned} \frac{d\langle \sigma_j^z \rangle(t)}{dt} &= \langle I_{j-1} \rangle(t) - \langle I_j \rangle(t) + \delta_{j,1} \Gamma [f - \langle \sigma_j^z \rangle(t)] \\ &\quad - \delta_{j,L} \Gamma [f + \langle \sigma_j^z \rangle(t)], \end{aligned} \quad (6)$$

involving the expectation value of the magnetization current $\langle I_j \rangle(t)$ flowing from j to $j + 1$, where Equation 7

$$I_j = \frac{2J}{\hbar} (\sigma_j^x \sigma_{j+1}^y - \sigma_j^y \sigma_{j+1}^x) \quad (7)$$

defines the corresponding current operator. Note that the dephasing reservoir does not change the average magnetization and therefore does not contribute explicitly to Equation 6, although it still affects the average magnetization and currents implicitly. Moreover, the boundary reservoirs do not contribute to the expression of the current in the bulk of the chain.

When the steady state is reached, the left-hand side of Equations 2, 6 vanishes. We denote by $\langle A \rangle_\infty \equiv \text{Tr}[A\rho(\infty)]$ the expectation value of A at the steady state $\rho(\infty)$. From Equation 6 we obtain Equations 8–10 for the steady-state current:

$$\langle I_1 \rangle_\infty = \Gamma(f - \langle \sigma_1^z \rangle_\infty), \tag{8}$$

$$\langle I_{j-1} \rangle_\infty = \langle I_j \rangle_\infty, \quad j = 2, 3, \dots, L-1 \tag{9}$$

$$\langle I_{L-1} \rangle_\infty = -\Gamma(f + \langle \sigma_L^z \rangle_\infty). \tag{10}$$

This current is uniform across the chain, with its value dictated by the average magnetization at the boundaries; from now on, we remove the subscript and denote it simply by $\langle I \rangle_\infty$. In the absence of any bias ($f = 0$), the boundary reservoirs induce an infinite temperature (maximally-mixed) steady state $\rho(\infty) = \mathbb{I}/2^L$, in which the values of magnetization and current all vanish.

2.2 Steady-state ansatz

In order to study the transport properties of the model at the steady state, both numerically and analytically, we make use of a perturbative ansatz characterized by an expansion in terms of potential bias f as [31, 32, 36].

$$\rho = \frac{1}{2^L} [\mathbb{I} + f(H + B) + \mathcal{O}(f^2)], \tag{11}$$

$$H = \sum_{r=1}^L \sum_{j=1}^{L+1-r} h_j^{(r)} H_j^{(r)}, \tag{12}$$

$$B = \sum_{r=2}^L \sum_{j=1}^{L+1-r} b_j^{(r)} B_j^{(r)}, \tag{13}$$

where $h_j^{(r)}$ and $b_j^{(r)}$ where in Equations 11–13 are expansion coefficients, and the corresponding operators are given by Equation 14

$$\begin{aligned} H_j^{(1)} &= -\sigma_j^z, \\ H_j^{(r)} &= \sigma_j^x Z_{j+1}^{(r-2)} \sigma_{j+r-1}^x + \sigma_j^y Z_{j+1}^{(r-2)} \sigma_{j+r-1}^y, \quad r \geq 2 \\ B_j^{(r)} &= \sigma_j^x Z_{j+1}^{(r-2)} \sigma_{j+r-1}^y - \sigma_j^y Z_{j+1}^{(r-2)} \sigma_{j+r-1}^x, \quad r \geq 2. \end{aligned} \tag{14}$$

These operators are thus strings of Pauli matrices starting at site j and having length r , where $Z_{k+1}^{(r-2)} = \sigma_{k+1}^z \sigma_{k+2}^z \dots \sigma_{k+r-3}^z \sigma_{k+r-2}^z$ are strings of Pauli z matrices of length $r-2$. The defining characteristic of this ansatz is that all operators in the expansion are orthogonal according to the Hilbert-Schmidt inner product $\langle A, B \rangle \equiv \text{Tr}[A^\dagger B]$. This implies that the expectation values of $H_j^{(r)}$ and $B_j^{(r)}$ are *exactly* determined within first order in f . In particular, $H_j^{(1)}$ and $B_j^{(2)}$ are respectively proportional to the magnetization and current

$$\langle \sigma_j^z \rangle_\infty = -f h_j^{(1)}, \quad \langle I_j \rangle_\infty = f \frac{4J b_j^{(2)}}{\hbar}. \tag{15}$$

Once we determine the first order expansion coefficients $h_j^{(r)}$ and $b_j^{(r)}$, we have access to the exact current and magnetization profile, as dictated by Equation 15 [32, 36, 38, 39]. In order to obtain them, we insert Equation 11 into Equation 2 and set the left-hand side to zero as demanded at stationarity (see Refs. Žnidarič [31]; Žnidarič and Horvat [32] and Supplementary Material for more details). This gives rise to a set of equations for the coefficients.

$$\hbar \Gamma(1 + h_1^{(1)}) - 4J b_1^{(2)} = 0, \tag{16}$$

$$\hbar \Gamma(1 - h_L^{(1)}) - 4J b_{L-1}^{(2)} = 0, \tag{17}$$

$$b_j^{(2)} - b_{j-1}^{(2)} = 0, \quad j = 2, \dots, L-1, \tag{18}$$

for $r = 1$. Note that Equations 16–18 just express the fact that the current is uniform in the steady state, with its value dictated by the boundary reservoirs as discussed before. For $r \geq 2$ we have.

$$\begin{aligned} J [h_j^{(r-1)} - h_{j+1}^{(r-1)} + h_j^{(r+1)} - h_{j-1}^{(r+1)}] + (\epsilon_j - \epsilon_{j+r-1}) h_j^{(r)} \\ + \hbar \left[\gamma + \frac{\Gamma}{4} (\delta_{j,1} + \delta_{j+r-1,L}) \right] b_j^{(r)} = 0, \end{aligned} \tag{19}$$

$$\begin{aligned} J [b_j^{(r-1)} - b_{j+1}^{(r-1)} + b_j^{(r+1)} - b_{j-1}^{(r+1)}] + (\epsilon_j - \epsilon_{j+r-1}) b_j^{(r)} \\ - \hbar \left[\gamma + \frac{\Gamma}{4} (\delta_{j,1} + \delta_{j+r-1,L}) \right] h_j^{(r)} = 0. \end{aligned} \tag{20}$$

In total, Equations 16–20 are a closed set of L^2 coupled equations and will be the starting point of our study. This set of equations is equivalent to a Lyapunov-type equation for the correlation matrix in the presence of dephasing [32]. Instead of the exponential scaling with the system size, the quadratic scaling makes the problem computationally tractable. Moreover, as we show below, it also allow us to find analytical expressions for the current under some mild assumptions.

3 Dephasing-assisted transport

We now discuss separately the effect of the tilt and dephasing on the transport properties of the model, while their interplay is addressed in the next section. The bias f of each reservoir at the boundaries induces transport along the chain. Intuitively, a similar effect is expected in the presence of an electric field which increases/decreases at each site at a rate U , or tilt between neighbour sites. If the tilt decreases from left to right, the local potentials are

$$\epsilon_j = -Uj. \tag{21}$$

Setting the bias to $f = 1$ drives excitations in the same direction (see Figure 1). Note that changing the sign of f inverts the sign of the current and magnetization, while changing the sign of U affects neither [39].

Since the tilt U represents the energy difference between nearest neighbours in the chain, the total tilt $V = U(L-1)$ represents the difference in energy across the whole chain. This quantity diverges in the thermodynamic limit, so that a physically meaningful analysis requires fixing the total tilt V and allowing U to decrease with the system size L . As discussed in Sections. 3.2 and 3.3, this procedure introduces a non-trivial dependence of the current with system size in the presence of dephasing: while for fixed U the current is expected to decrease with the system size L , this will no longer be the case for fixed V .

Such a linear potential is known to induce Wannier-Stark localization in the absence of dephasing, with U/\hbar being the frequency of Bloch oscillations [20–22, 24]. In the absence of dephasing $\gamma = 0$ and for non-vanishing tilt $V > 0$, the steady state magnetization profile shows the formation of domain walls [39] – regions of constant magnetization $\langle \sigma_j^z \rangle_\infty \approx \pm f$ starting at the boundaries and extending inwards as shown in Figure 2A. According to Equation 8 or Equation 10, this implies a vanishing current, which characterizes the localized system. Indeed we observe in Figure 2B that, as V increases, the current displays an exponential decay with the system size $\langle I \rangle_\infty \sim e^{-L/L_0}$ with L_0 being the

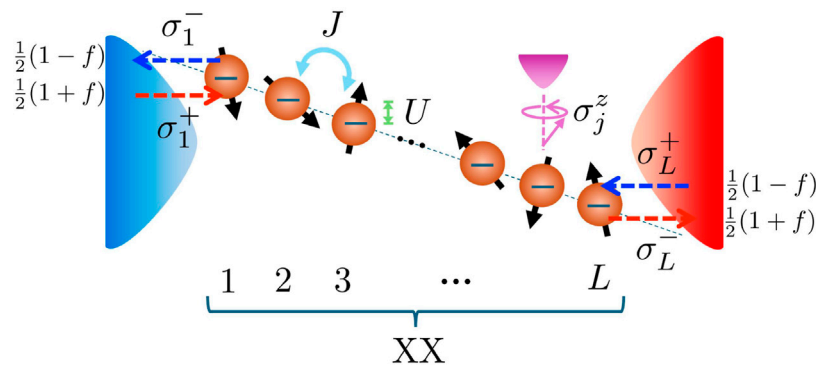


FIGURE 1
A schematic diagram of the system under study. The lattice is modeled as an XX spin chain, characterised by a hopping amplitude J and on-site field linearly decaying in steps of U across the chain. The boundary sites are coupled to separate reservoirs that inject/eject spin excitations controlled by a bias f , while in the bulk each spin is coupled to its own local reservoir which induces dephasing.

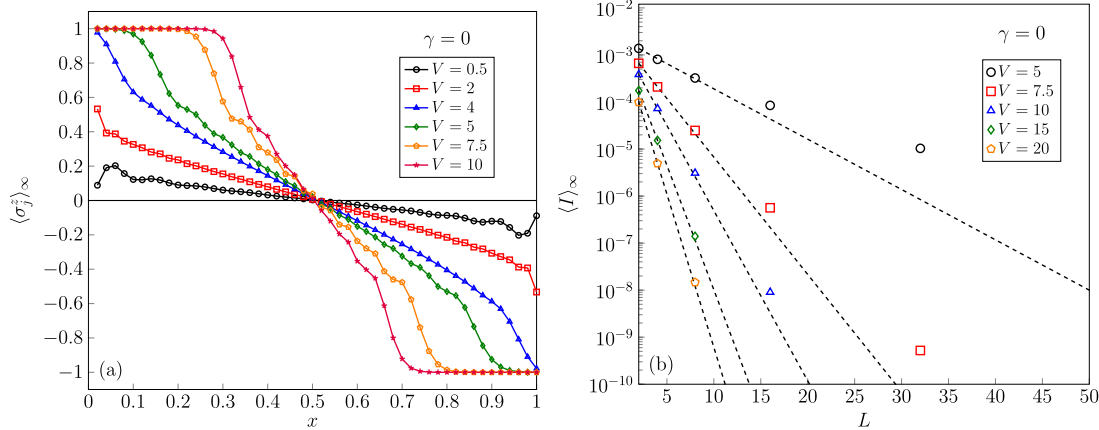


FIGURE 2
(A) Steady-state magnetization profile $\{\langle \sigma_j^z \rangle_\infty\}_{j=1}^L$ for system size $L = 50$ and different values of total tilt V . The site positions are normalized $x = j/L$. **(B)** Steady-state current $\langle I \rangle_\infty$ as a function of system size for different values of total tilt V . The dashed lines represent exponential fits $\langle I \rangle_\infty \propto e^{-L/L_0}$ to the data with $L_0 = 4.06, 1.75, 1.20, 0.82, 0.67$ respectively for $V = 5, 7.5, 10, 15, 20$. Parameters: $\hbar = f = J = 1$, $\Gamma = 0.01$ and $\gamma = 0$.

localization length. Note that L_0 here is different from the localization region of a single particle in a Wannier-Stark localized system given by J/U [22].

The results in the absence of tilt $U = V = 0$ are shown in Figures 3, 5A, respectively for the magnetization and the current. We distinguish two regimes: $\gamma = 0$ and $\gamma > 0$. The first case corresponds to ballistic transport, characterized by a small (but non-zero) magnetization at the boundaries and zero bulk magnetization (inset of Figure 3), together with a size-independent current (see later Figure 5A). The second case corresponds to diffusive transport, characterized by an emerging linear magnetization profile as the dephasing rate increases, accompanied by a decreasing current in accordance with Equation 8, 10. For very large dephasing or system sizes the current scales as $\langle I \rangle_\infty \sim 1/(\gamma L)$ signaling diffusive transport. The exact expression for the current in the absence of tilt is given by Equation 30 (with $U = V = 0$) as we discuss in Sec. 3.2.

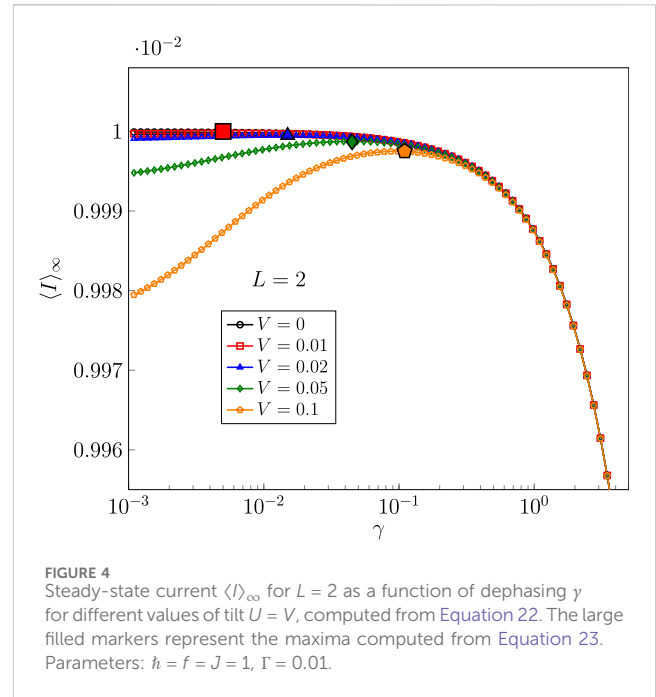
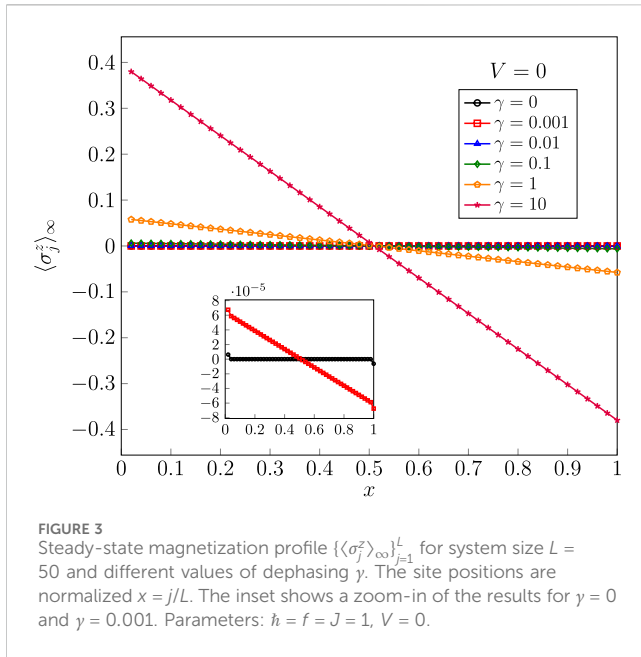
3.1 Exact current for small system sizes

Having shown the degrading effect of the tilt and dephasing separately on the spin transport across the system, we now study their interplay which gives rise to dephasing-enhanced transport. In this section, we focus on transport for small system sizes $L = 2, 3$. An exact and compact solution for the current can be found from Equations 16–20 in these cases. For $L = 2$ we obtain

$$\langle I \rangle_\infty = f \frac{16J^2\Gamma(2\gamma + \Gamma)}{16J^2(2\gamma + \Gamma) + 4\Gamma U^2 + \hbar^2\Gamma(2\gamma + \Gamma)^2}. \quad (22)$$

Dephasing-assisted transport can be characterised through the maximum of Equation 22 with respect to the dephasing rate γ , yielding an optimal dephasing rate

$$\gamma_{\max} = \frac{U}{\hbar} - \frac{\Gamma}{2} \geq 0. \quad (23)$$



The behaviour of Equation 22 is shown in Figure 4. Note that since the dephasing is always positive, the maximum only occurs if $U/\hbar \geq \Gamma/2$.

For $L = 3$ we have a similar expression, namely,

$$\langle I \rangle_\infty = f \frac{16J^2\Gamma(4\gamma + \Gamma)}{16J^2(4\gamma + \Gamma) + 16\Gamma U^2 + \hbar^2\Gamma(4\gamma + \Gamma)^2} \quad (24)$$

where the maximum is given by Equation 25

$$\gamma_{\max} = \frac{U}{\hbar} - \frac{\Gamma}{4} \geq 0. \quad (25)$$

The complexity of these expressions increases rapidly for $L > 3$, so the exact evaluation of the current and its maximum is too involved to be displayed here for larger systems. In the following section, we resort to an approximate solution for the current.

3.2 Tridiagonal approximation

In order to find an exact solution for systems of arbitrary size, we perform the *tridiagonal approximation* which consists of retaining strings of Pauli matrices up to $r = 2$, that is, ignoring higher order coefficients in Equations 16–20 so that $h_j^{(r)}, b_j^{(r)} = 0$ for $r \geq 3$. In the correlation matrix approach, this is equivalent to retaining only the diagonal and first off-diagonal elements [32]. Physically, this implies that spin and current correlations can be ignored within first order in f , which allows the derivation of an exact expression for the current as a function of all parameters as we now show. We only have to consider Equations 19, 20 for $r = 2$. Summing Equation 19 from $j = 1$ to $j = L - 1$ we obtain

$$J(h_1^{(1)} - h_L^{(1)}) + \sum_{j=1}^{L-1} (\epsilon_j - \epsilon_{j+1})h_j^{(2)} + \hbar b[\gamma(L - 1) + \Gamma/4] = 0, \quad (26)$$

where $b \equiv b_j^{(2)}$ is the coefficient associated with the current, which is independent of j as a consequence of Equation 18. First, we can write $h_1^{(1)} - h_L^{(1)}$ as a function of b by using Equations 16, 17, which yields

$$h_1^{(1)} - h_L^{(1)} = \frac{8Jb}{\hbar\Gamma} - 2. \quad (27)$$

Second, we can also express $h_j^{(2)}$ as a function of b by using Equation 20, which leads to Equation 28

$$h_j^{(2)} = \frac{(\epsilon_j - \epsilon_{j+1})b}{\hbar[\gamma + (\delta_{j,1} + \delta_{j,L-1})\Gamma/4]}. \quad (28)$$

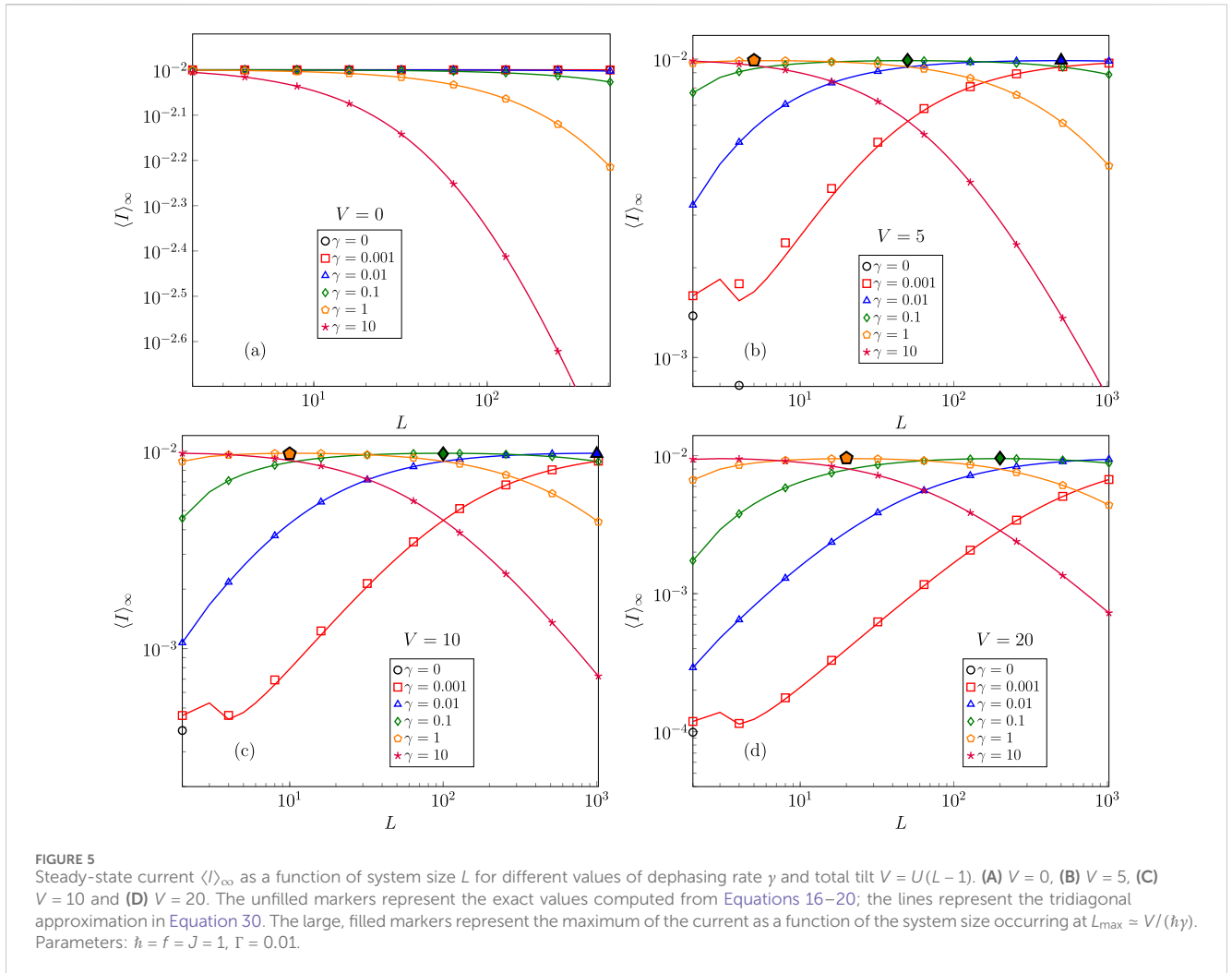
We can now substitute the previous two equations into Equation 26 and obtain an expression for b , namely,

$$b = \frac{4J}{2\hbar\gamma(L - 1) + \hbar\Gamma + \frac{16J^2}{\hbar\Gamma} + 2\sum_{j=1}^{L-1} \frac{(\epsilon_j - \epsilon_{j+1})^2}{\gamma + (\delta_{j,1} + \delta_{j,L-1})\Gamma/4}}. \quad (29)$$

The current is now obtained from Equations 15 and 29. For the local tilted potential in Equation 21 it becomes

$$\langle I \rangle_\infty = f \frac{16J^2\Gamma}{16J^2 + \hbar^2\Gamma[\Gamma + 2\gamma(L - 1)] + 4\Gamma U^2} \begin{cases} 1/(2\gamma + \Gamma) & L = 2 \\ (L - 3)/(2\gamma) + 4/(4\gamma + \Gamma) & L \geq 3 \end{cases} \quad (30)$$

We note that this expression is exact for $L = 2$ and $L = 3$, in which case we recover Equations 22, 24, respectively. It is also exact in the absence of tilt $U = V = 0$ [31, 32, 37], which is verified in Figure 5A. In Figures 5B–D we plot the exact solution and the tridiagonal approximation for non-zero values of total tilt $V > 0$. We observe that the approximation works remarkably well, deviating from the exact solution only for very small dephasing rates and system sizes; when $\gamma = 0$, the approximation fails dramatically and



only the exact solution is shown. The latter case corresponds to a Wannier-Stark localized system which we already discussed. Moreover, we see that for fixed γ the current can now increase with the system size up to a critical size L_{\max} where it is maximal, and only then decreases. In the same way, we see that for fixed L there is a critical dephasing rate γ_{\max} at which the current is maximal.

3.3 Interplay between dephasing and tilt

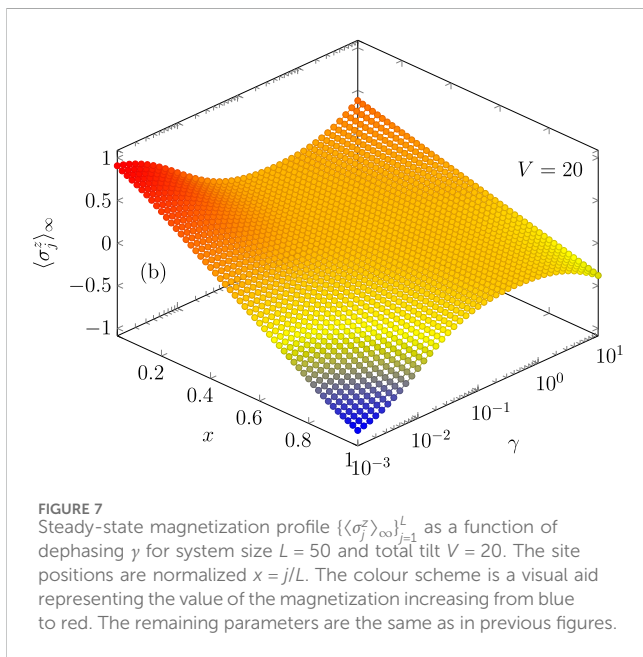
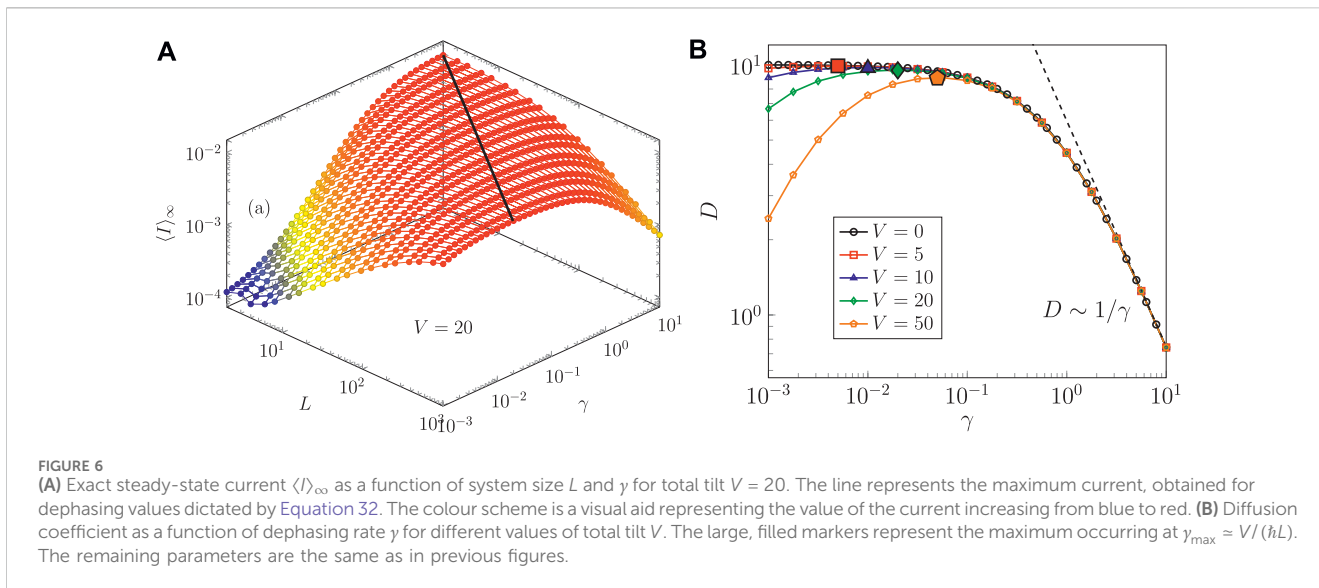
Since the validity of Equation 30 is established, we now use it to determine both L_{\max} and γ_{\max} . The maxima of Equation 30 as a function of L (for fixed V and γ) and γ (for fixed L and V) can be determined exactly. However, as before, the expressions are too lengthy to be displayed. More physically intuitive expressions are obtained by assuming that $L \gg 1$ and $L \gg 8\gamma/(4\gamma + \Gamma)$ in the denominator of Equation 30 which leads to the approximate maxima.

$$L_{\max} \approx \frac{V}{\hbar\gamma}, \tag{31}$$

$$\gamma_{\max} \approx \frac{V}{\hbar L} = \frac{U}{\hbar}. \tag{32}$$

These maxima characterize dephasing-assisted transport as we show in Figure 6A. Below the critical length ($L_{\max} \gg L \gg 1$), dephasing is not yet effective and an increase in L decreases the local tilt $U = V/(L - 1)$ and thus localization, which increases the current according to Equation 30. Above this length scale ($L \gg L_{\max} \gg 1$) dephasing becomes effective and diffusive transport clearly emerges ($\langle I \rangle_\infty \sim 1/(\gamma L)$). Analogously, below the critical dephasing rate ($\gamma_{\max} \gg \gamma$) dephasing jump events happen at a much lower frequency than Bloch oscillations, so the current flowing remains hampered by localization. Increasing the rate of dephasing destroys localization and increases the current. When the dephasing rate passes this threshold ($\gamma \gg \gamma_{\max}$) diffusive behaviour emerges. We illustrate this in Figure 6B where we plot the (finite size) diffusion coefficient defined by $\langle I \rangle_\infty \equiv fD/L$ as a function of dephasing rate for the largest system size we reached $L = 1000$.

The imprint of dephasing-enhanced transport is also evident in the magnetization profile, as shown in Figure 7. Here, varying the dephasing strength towards its critical value Equation 32 decreases the magnetization gradient, rendering the magnetization profile almost uniform. This is in contrast with the results obtained in the absence of tilt, where an increasing dephasing rate tends to increase the magnetization gradient and decrease uniformity as shown in Figure 3A. Uniformity as a feature of environment-



assisted transport has been pointed out for quantum systems subject to on-site disorder [9]; our results confirm that the same phenomenon appears in the presence of a linear potential inducing Wannier-Stark localization.

4 Conclusion and outlook

In this paper, we have exploited an exact ansatz to obtain the steady state of a non-interacting spin chain subject to bulk dephasing, a linear potential and boundary-driving. This description has allowed us to unravel the delicate interplay between Wannier-Stark localization and dephasing-induced diffusive transport. We applied the tridiagonal approximation, where only on-site and nearest-

neighbour correlation matrix elements are retained, to derive an approximate expression for the steady-state current as a function of both dephasing and tilt. This expression is found to closely match the exact solution for a wide range of parameters, and reveals that the maximum current occurs for a dephasing rate equal to the period of Bloch oscillations in the Wannier-Stark localized system. Fixing the total tilt across the system then revealed a maximum in the current as a function of system size. This evidences a critical system size beyond which Bloch oscillations are suppressed by dephasing.

Our work motivates future analytical and numerical analysis on the interplay between dephasing and a tilted potential in more complex and richer systems, e.g., those including interactions between neighboring sites [40–42], time-periodic driving [43, 44], or more realistic (non-Markovian) boundary-driving schemes [45–50]. Another promising research avenue is to study the sensing capacity of our quantum many-body system. Indeed, it has been recently shown that the non-equilibrium dynamics of Bloch oscillations can enhance the sensing capacity of an isolated quantum many-body system [51]; it would be interesting to examine whether such an advantage is found for a quantum many-body system subject to dephasing, particularly in the dephasing-assisted transport regime. Finally, our results can be readily verified in current photonic [52], ion-trap [53] and cold-atom [54–56] experimental platforms.

Data availability statement

The original contributions presented in the study are included in the article/Supplementary Material, further inquiries can be directed to the corresponding author.

Author contributions

SJ: Writing—original draft, Writing—review and editing. LB: Writing—original draft, Writing—review and editing. AL:

Writing—original draft, Writing—review and editing. KZ: Writing—original draft, Writing—review and editing. SC: Writing—original draft, Writing—review and editing. JG: Writing—original draft, Writing—review and editing. JM-A: Writing—original draft, Writing—review and editing.

Funding

The author(s) declare that financial support was received for the research, authorship, and/or publication of this article. The authors declare financial support was received for the research, authorship, and/or publication of this article. S.L.J. acknowledges the financial support from a Marie Skłodowska-Curie Fellowship (Grant No. 101103884). S.R.C. gratefully acknowledge financial support from UK's Engineering and Physical Sciences Research Council (EPSRC) under grant EP/T028424/1 which is part of an EPSRC-SFI joint project QuamNESS funded also by the SFI under the Frontier For the Future Program. JG is supported by a SFI Royal Society University Research Fellowship.

References

- Joos E, Zeh HD, Kiefer C, Giulini D, Kupsch J, Stamatescu I-O. *Decoherence and the appearance of a classical world in quantum theory*. Springer Berlin Heidelberg (2003). doi:10.1007/978-3-662-05328-7
- Breuer H-P, Petruccione F. *The theory of open quantum systems*. Oxford University Press (2007).
- Rivas Á, Huelga SF. *Open quantum systems*. Springer Berlin Heidelberg (2012). doi:10.1007/978-3-642-23354-8
- Plenio MB, Huelga SF. Dephasing-assisted transport: quantum networks and biomolecules. *New J Phys* (2008) 10:113019. doi:10.1088/1367-2630/10/11/113019
- Mohseni M, Rebentrost P, Lloyd S, Aspuru-Guzik A. Environment-assisted quantum walks in photosynthetic energy transfer. *J Chem Phys* (2008) 129:174106. doi:10.1063/1.3002335
- Rebentrost P, Mohseni M, Kassel I, Lloyd S, Aspuru-Guzik A. Environment-assisted quantum transport. *New J Phys* (2009) 11:033003. doi:10.1088/1367-2630/11/3/033003
- Chin AW, Datta A, Caruso F, Huelga SF, Plenio MB. Noise-assisted energy transfer in quantum networks and light-harvesting complexes. *New J Phys* (2010) 12:065002. doi:10.1088/1367-2630/12/6/065002
- Sinayskiy I, Marais A, Petruccione F, Ekert A. Decoherence-assisted transport in a dimer system. *Phys Rev Lett* (2012) 108:020602. doi:10.1103/physrevlett.108.020602
- Zerah-Harush E, Dubi Y. Effects of disorder and interactions in environment assisted quantum transport. *Phys Rev Res* (2020) 2:023294. doi:10.1103/physrevresearch.2.023294
- Zerah-Harush E, Dubi Y. Do photosynthetic complexes use quantum coherence to increase their efficiency? probably not. *Sci Adv* (2021) 7:eabc4631. doi:10.1126/sciadv.abc4631
- Alterman S, Berman J, Strauch FW. Optimal conditions for environment-assisted quantum transport on the fully connected network. *Phys Rev E* (2024) 109:014310. doi:10.1103/physreve.109.014310
- Ferreira J, Jin T, Mannhart J, Giamarchi T, Filippone M. Transport and nonreciprocity in monitored quantum devices: an exact study. *Phys Rev Lett* (2024) 132:136301. doi:10.1103/physrevlett.132.136301
- Viciani S, Lima M, Bellini M, Caruso F. Observation of noise-assisted transport in an all-optical cavity-based network. *Phys Rev Lett* (2015) 115:083601. doi:10.1103/physrevlett.115.083601
- Tang H, Shang X-W, Shi Z-Y, He T-S, Feng Z, Wang T-Y, et al. Simulating photosynthetic energy transport on a photonic network. *Npj Quan Inf* (2024) 10:29. doi:10.1038/s41534-024-00824-x
- Gorman DJ, Hemmerling B, Megidish E, Moeller SA, Schindler P, Sarovar M, et al. Engineering vibrationally assisted energy transfer in a trapped-ion quantum simulator. *Phys Rev X* (2018) 8:011038. doi:10.1103/physrevx.8.011038

Conflict of interest

The authors declare that the research was conducted in the absence of any commercial or financial relationships that could be construed as a potential conflict of interest.

Publisher's note

All claims expressed in this article are solely those of the authors and do not necessarily represent those of their affiliated organizations, or those of the publisher, the editors and the reviewers. Any product that may be evaluated in this article, or claim that may be made by its manufacturer, is not guaranteed or endorsed by the publisher.

Supplementary material

The Supplementary Material for this article can be found online at: <https://www.frontiersin.org/articles/10.3389/fphy.2024.1474018/full#supplementary-material>

- Maier C, Brydges T, Jurcevic P, Trautmann N, Hempel C, Lanyon BP, et al. Environment-assisted quantum transport in a 10-qubit network. *Phys Rev Lett* (2019) 122:050501. doi:10.1103/physrevlett.122.050501
- Potočník A, Bargerbos A, Schröder FAYN, Khan SA, Collodo MC, Gasparinetti S, et al. Studying light-harvesting models with superconducting circuits. *Nat Comm* (2018) 9:904. doi:10.1038/s41467-018-03312-x
- Anderson PW. Absence of diffusion in certain random lattices. *Phys Rev* (1958) 109:1492–505. doi:10.1103/physrev.109.1492
- Bloch F. Über die quantenmechanik der elektronen in kristallgittern. *Z Physik* (1929) 52:555–600. doi:10.1007/bf01339455
- Zener C. A theory of the electrical breakdown of solid dielectrics. *Proc R Soc Lond A* (1934) 145:523–9. doi:10.1098/rspa.1934.0116
- Wannier GH. Dynamics of band electrons in electric and magnetic fields. *Rev Mod Phys* (1962) 34:645–55. doi:10.1103/revmodphys.34.645
- Hartmann T, Keck F, Korsch HJ, Mossmann S. Dynamics of bloch oscillations. *New J Phys* (2004) 6:2. doi:10.1088/1367-2630/6/1/002
- van Nieuwenburg E, Baum Y, Refael G. From bloch oscillations to many-body localization in clean interacting systems. *PNAS* (2019) 116:9269–74. doi:10.1073/pnas.1819316116
- Guo X-Y, Ge ZY, Li H, Wang Z, Zhang Y-R, Song P, et al. Observation of bloch oscillations and wannier-Stark localization on a superconducting quantum processor. *Npj Quan Inf* (2021) 7:51. doi:10.1038/s41534-021-00385-3
- Burkhardt S, Kraft M, Mannella R, Wimberger S. Noise-assisted transport in the wannier-Stark system. *New J Phys* (2013) 15:045008. doi:10.1088/1367-2630/15/4/045008
- Bhakuni DS, Dattagupta S, Sharma A. Effect of noise on bloch oscillations and wannier-Stark localization. *Phys Rev B* (2019) 99:155149. doi:10.1103/PhysRevB.99.155149
- Langlett CM, Xu S. Noise-induced universal diffusive transport in fermionic chains. *Phys Rev B* (2023) 108:1180303. doi:10.1103/physrevb.108.1180303
- Teretenkov A, Lychkovskiy O. Exact dynamics of quantum dissipative XX models: wannier-Stark localization in the fragmented operator space. *Phys Rev B* (2024) 109: L140302. doi:10.1103/PhysRevB.109.L140302
- Bertini B, Heidrich-Meisner F, Karrasch C, Prosen T, Steinigeweg R, Žnidarič M. Finite-temperature transport in one-dimensional quantum lattice models. *Rev Mod Phys* (2021) 93:025003. doi:10.1103/revmodphys.93.025003
- Landi GT, Poletti D, Schaller G. Nonequilibrium boundary-driven quantum systems: models, methods, and properties. *Rev Mod Phys* (2022) 94:045006. doi:10.1103/revmodphys.94.045006
- Žnidarič M. Dephasing-induced diffusive transport in the anisotropic heisenberg model. *New J Phys* (2010) 12:043001. doi:10.1088/1367-2630/12/4/043001
- Žnidarič M, Horvat M. Transport in a disordered tight-binding chain with dephasing. *Eur Phys J B* (2013) 86:67. doi:10.1140/epjb/e2012-30730-9

33. Žnidarič M, Mendoza-Arenas JJ, Clark SR, Goold J. Dephasing enhanced spin transport in the ergodic phase of a many-body localizable system. *Annalen der Physik* (2016) 529:1600298. doi:10.1002/andp.201600298
34. Lacerda AM, Goold J, Landi GT. Dephasing enhanced transport in boundary-driven quasiperiodic chains. *Phys Rev B* (2021) 104:174203. doi:10.1103/physrevb.104.174203
35. Sarkar S, Agarwalla BK, Bhakuni DS. Impact of dephasing on nonequilibrium steady-state transport in fermionic chains with long-range hopping. *Phys Rev B* (2024) 109:165408. doi:10.1103/physrevb.109.165408
36. Žnidarič M. Solvable quantum nonequilibrium model exhibiting a phase transition and a matrix product representation. *Phys Rev E* (2011) 83:011108. doi:10.1103/physreve.83.011108
37. Turkeshi X, Schiró M. Diffusion and thermalization in a boundary-driven dephasing model. *Phys Rev B* (2021) 104:144301. doi:10.1103/physrevb.104.144301
38. Žnidarič M. Exact solution for a diffusive nonequilibrium steady state of an open quantum chain. *J Stat Mech* (2010) 2010:L05002. doi:10.1088/1742-5468/2010/05/L05002
39. Mendoza-Arenas JJ, Clark SR. Giant rectification in strongly interacting driven tilted systems. *PRX Quantum* (2024) 5:010341. doi:10.1103/PRXQuantum.5.010341
40. Mendoza-Arenas JJ, Grujic T, Jaksch D, Clark SR. Dephasing enhanced transport in nonequilibrium strongly correlated quantum systems. *Phys Rev B* (2013) 87:235130. doi:10.1103/PhysRevB.87.235130
41. Mendoza-Arenas JJ, Al-Assam S, Clark SR, Jaksch D. Heat transport in the XXZ spin chain: from ballistic to diffusive regimes and dephasing enhancement. *J Stat Mech* (2013) 2013:P07007. doi:10.1088/1742-5468/2013/07/P07007
42. Mendoza-Arenas JJ, Mitchison MT, Clark SR, Prior J, Jaksch D, Plenio MB. Transport enhancement from incoherent coupling between one-dimensional quantum conductors. *New J Phys* (2014) 16:053016. doi:10.1088/1367-2630/16/5/053016
43. De B, Wójtowicz G, Zakrzewski J, Zwolak M, Rams MM. Transport in a periodically driven tilted lattice via the extended reservoir approach: stability criterion for recovering the continuum limit. *Phys Rev B* (2023) 107:235148. doi:10.1103/PhysRevB.107.235148
44. De B, Wójtowicz G, Rams MM, Zwolak M, Zakrzewski J. *The confluence of fractured resonances at points of dynamical, many-body flare*. arXiv:2308.12346 (2024).
45. Prior J, Chin AW, Huelga SF, Plenio MB. Efficient simulation of strong system-environment interactions. *Phys Rev Lett* (2010) 105:050404. doi:10.1103/PhysRevLett.105.050404
46. Tamascelli D, Smirne A, Huelga SF, Plenio MB. Nonperturbative treatment of non-markovian dynamics of open quantum systems. *Phys Rev Lett* (2018) 120:030402. doi:10.1103/PhysRevLett.120.030402
47. Strathearn A, Kirton P, Kilda D, Keeling J, Lovett BW. Efficient non-markovian quantum dynamics using time-evolving matrix product operators. *Nat Comm* (2018) 9:3322. doi:10.1038/s41467-018-05617-3
48. Brenes M, Mendoza-Arenas JJ, Purkayastha A, Mitchison MT, Clark SR, Goold J. Tensor-network method to simulate strongly interacting quantum thermal machines. *Phys Rev X* (2020) 10:031040. doi:10.1103/PhysRevX.10.031040
49. Purkayastha A, Guarnieri G, Campbell S, Prior J, Goold J. Periodically refreshed baths to simulate open quantum many-body dynamics. *Phys Rev B* (2021) 104:045417. doi:10.1103/PhysRevB.104.045417
50. Anto-Sztrikacs N, Nazir A, Segal D. Effective-Hamiltonian theory of open quantum systems at strong coupling. *PRX Quantum* (2023) 4:020307. doi:10.1103/PRXQuantum.4.020307
51. Manshoury H, Zarei M, Abdi M, Bose S, Bayat A. *Quantum enhanced sensitivity through many-body bloch oscillations*. arXiv:2406.13921 (2024).
52. Ma R, Saxberg B, Owens C, Leung N, Lu Y, Simon J, et al. A dissipatively stabilized Mott insulator of photons. *Nature* (2019) 566:51–7. doi:10.1038/s41586-019-0897-9
53. Morong W, Liu F, Becker P, Collins K, Feng L, Kyprianidis A, et al. Observation of Stark many-body localization without disorder. *Nature* (2021) 599:393–8. doi:10.1038/s41586-021-03988-0
54. Krinner S, Esslinger T, Brantut J-P. Two-terminal transport measurements with cold atoms. *J Phys Condens Matter* (2017) 29:343003. doi:10.1088/1361-648x/aa74a1
55. Scherg S, Kohler T, Sala P, Pollmann F, Hebbe Madhusudhana B, Bloch I, et al. Observing non-ergodicity due to kinetic constraints in tilted Fermi-Hubbard chains. *Nat Comm* (2021) 12:4490. doi:10.1038/s41467-021-24726-0
56. Amico L, Anderson D, Boshier M, Brantut J-P, Kwek L-C, Minguzzi A, et al. Colloquium: atomtronic circuits: from many-body physics to quantum technologies. *Rev Mod Phys* (2022) 94:041001. doi:10.1103/RevModPhys.94.041001